

# Panic contagion and the evacuation dynamics

F.E. Cornes<sup>a</sup>, G.A. Frank<sup>c</sup>, C.O. Dorso<sup>a,b</sup>

<sup>a</sup>Departamento de Física, Facultad de Ciencias Exactas y Naturales, Universidad de Buenos Aires, Pabellón I, Ciudad Universitaria, 1428 Buenos Aires, Argentina.

<sup>b</sup>Instituto de Física de Buenos Aires, Pabellón I, Ciudad Universitaria, 1428 Buenos Aires, Argentina.

<sup>c</sup> Unidad de Investigación y Desarrollo de las Ingenierías, Universidad Tecnológica Nacional, Facultad Regional Buenos Aires, Av. Medrano 951, 1179 Buenos Aires, Argentina.

---

## Abstract

Panic may spread over a crowd in a similar fashion as contagious diseases do in social groups. People exposed directly to a panic source may express fear, alerting others of imminent danger. This social mechanism initiates an evacuation process, while affecting the way people try to escape. We examined real life situations of panic contagion and reproduced these situations in the context of the Social Force Model. We arrived to the conclusion that two evacuation schemes may appear, according to the pedestrian susceptibility to get into panic. Both schemes exhibit different evacuation patterns and are qualitatively visible in the available real life recordings of crowded events. We quantified these patterns through topological parameters. We further investigated how the panic spreading gradually stops if the source of danger ceases.

*Keywords:*

Emergency evacuation, Social force model, Panic spreading

*PACS:* 45.70.Vn, 89.65.Lm

---

## <sup>1</sup> 1. Introduction

<sup>2</sup> Many authors called the attention on the fact that panic is a contagious  
<sup>3</sup> phenomenon [1, 2, 3, 4]. Panic may spread over any “social group” if some  
<sup>4</sup> kind of coupling mechanism exists between agents [1]. This coupling mecha-  
<sup>5</sup> nism corresponds to social communication between the members of the group.  
<sup>6</sup> As a consequence, the individuals (agents) may change their anxiety state

7 from relaxed to a panic one (and back again) [1].

8

9 Panic contagion over the crowd can be attained if the coupling mech-  
10 anism between individuals is strong enough and affects many neighboring  
11 pedestrians [1]. Research on random lattices shows that the coupling stress  
12 becomes relevant whenever the number on neighbors is small (*i.e.* less than  
13 four). That is, a small connectivity number between agents (pedestrians)  
14 requires really moving gestures [1].

15

16 Recent investigation suggests that other psychological mechanisms than  
17 social communication can play an important role during the panic spreading  
18 over the crowd [2, 3, 5]. Susceptibility appear as relevant attributes that  
19 control the panic propagation [2]. Consequently, diseases contagion models  
20 are usually introduced when studying the panic spreading. The Susceptible-  
21 Infected-Recovered-Susceptible (SIRS) model raises as a suitable research  
22 tool for examining the panic dynamics. The spreading model is, therefore,  
23 represented as a system of first order equations [2, 5].

24

25 According to the SIRS model implemented in Ref. [2], a dramatic conta-  
26 gion of panic can be expected in those crowded situations where the individ-  
27 uals are not able to calm down quickly. The speed at which the individual  
28 calms down may not only depend on the current environment, but on other  
29 psychological attributes [2]. Ref. [6] proposes a characteristic value for this  
30 “stress decay”.

31

32 Although the SIRS model appears to be a reasonable approach to panic  
33 spreading, it has been argued that it may not accurately resemble the sit-  
34 uations of crowds with moving pedestrians [3, 4]. The moving pedestrians  
35 will get into panic if their “inner stress” exceeds a threshold [4]. That is, if  
36 the cumulative emotions received by the pedestrian’s neighbors surpasses a  
37 certain “inner stress” threshold.

38

39 Conversely, unlike the SIRS model, any panicking pedestrian may relax  
40 after some time due to “stress decay” (if no emotions of fear are received by  
41 the corresponding neighbors) [3, 4]. That is, in this case, there is not a prob-  
42 ability to switch from the anxious (infected) state to the relaxed (recovered)  
43 state as in the SIRS model, but a natural decay. Thus, the increase in the  
44 “inner stress” and the “stress decay” are actually the two main phenomena

45 determining the pedestrians behavior.

46

47 Researchers seem not to agree on how the increase in the “inner stress”  
48 and the “stress decay” affect the pedestrians behavioral patterns [7, 4, 8].  
49 Pelechano and co-workers [7] suggest that the maximum *current* velocity of  
50 the pedestrians may increase if he (she) gets into panic. But Fu and co-  
51 workers [4] propose to update the *desired* velocity (not the current one) of  
52 the pedestrian, according to his (her) current “inner stress” (see Section 2  
53 for details). Both investigations assume that the pedestrians move in the  
54 context of the Social Force Model (SFM).

55

56 More experimental data needs to be examined before arriving to consen-  
57 sus on how the panic contagion affects the pedestrians dynamics.

58

59 Our investigation focuses on two real life situations. Our aim is to de-  
60 velop a model for describing the panic contagion mechanism, where many  
61 individuals may suddenly switch to an anxious state. We will focus on video  
62 analyses in order to obtain reliable parameters from a real panic-contagion  
63 events, and further test these parameters on computer simulations.

64

65 In Section 2 we introduce the dynamic equations for evacuating pedes-  
66 trians, in the context of the Social Force Model (SFM). We also define the  
67 meaning of the appearance to danger, the *contagion stress* and their relation  
68 to the pedestrians desired velocity.

69

70 In Section 3 we present the real life situations considered in our investiga-  
71 tion. The corresponding simulations (in the SFM context) resembling these  
72 situations are detailed in Section 4.

73

74 Section 5 displays the results of our investigations, while some preliminary  
75 outcomes are summarized. Section 6 details the corresponding conclusions.

76

## 77 2. Background

### 78 2.1. The social force model

79 This investigation handles the pedestrians dynamics in the context of  
80 the “social force model” (SFM) [9]. The SFM exploits the idea that human

81 motion depends on the people's own desire to reach a certain destination at  
 82 a given velocity, as well as other environmental factors [10]. The former is  
 83 modeled by a force called the "desire force", while the latter is represented  
 84 by social forces and "granular forces". These forces enter the equation of  
 85 motion as follows

$$m_i \frac{d\mathbf{v}^{(i)}}{dt} = \mathbf{f}_d^{(i)} + \sum_{j=1}^N \mathbf{f}_s^{(ij)} + \sum_{j=1}^N \mathbf{f}_g^{(ij)} \quad (1)$$

86 where the  $i, j$  subscripts correspond to any two pedestrians in the crowd.  
 87  $\mathbf{v}^{(i)}(t)$  means the current velocity of the pedestrian ( $i$ ), while  $\mathbf{f}_d$  and  $\mathbf{f}_s$  cor-  
 88 respond to the "desired force" and the "social force", respectively.  $\mathbf{f}_g$  is the  
 89 friction or granular force.

90

91 The  $\mathbf{f}_d$  describes the pedestrians own desire to reach a specific target  
 92 position at the desired velocity  $v_d$ . But, due to environmental factors (*i.e.*  
 93 obstacles, visibility), he (she) actually moves at the current velocity  $\mathbf{v}^{(i)}(t)$ .  
 94 Thus, he (she) will accelerate (or decelerate) to reach any desired velocity  
 95  $v_d$  that will make him (her) feel more comfortable. Thus, in the social force  
 96 model, the desired force reads [9]

$$\mathbf{f}_d^{(i)}(t) = m_i \frac{v_d^{(i)} \mathbf{e}_d^{(i)}(t) - \mathbf{v}^{(i)}(t)}{\tau} \quad (2)$$

97 where  $m_i$  is the mass of the pedestrian  $i$  and  $\tau$  represents the relaxation  
 98 time needed to reach the desired velocity.  $\mathbf{e}_d$  is the unit vector pointing to  
 99 the target position. Detailed values for  $m_i$  and  $\tau$  can be found in Refs. [9, 11].

100

101 The "social force"  $\mathbf{f}_s(t)$  represents the socio-psychological tendency of  
 102 the pedestrians to preserve their *private sphere*. The spatial preservation  
 103 means that a repulsive feeling exists between two neighboring pedestrians, or,  
 104 between the pedestrian and the walls [9, 10]. This repulsive feeling becomes  
 105 stronger as people get closer to each other (or to the walls). Thus, in the  
 106 context of the social force model, this tendency is expressed as

$$\mathbf{f}_s^{(ij)} = A_i e^{(r_{ij} - d_{ij})/B_i} \mathbf{n}_{ij} \quad (3)$$

107 where  $(ij)$  corresponds to any two pedestrians, or to the pedestrian-wall in-  
 108 teraction.  $A_i$  and  $B_i$  are two fixed parameters (see Ref. [12]). The distance

109  $r_{ij} = r_i + r_j$  is the sum of the pedestrians radius, while  $d_{ij}$  is the distance  
 110 between the center of mass of the pedestrians  $i$  and  $j$ .  $\mathbf{n}_{ij}$  means the unit  
 111 vector in the  $\vec{ji}$  direction. For the case of repulsive feelings with the walls,  
 112  $d_{ij}$  corresponds to the shortest distance between the pedestrian and the wall,  
 113 while  $r_{ij} = r_i$  [9, 10].  
 114

115 It is worth mentioning that the Eq. (3) is also valid if two pedestrians are  
 116 in contact (*i.e.*  $r_{ij} > d_{ij}$ ), but its meaning is somehow different. In this case,  
 117  $\mathbf{f}_s$  represents a body repulsion, as explained in Ref. [13].  
 118

119 The granular force  $\mathbf{f}_g$  included in Eq. (1) corresponds to the sliding friction  
 120 between pedestrians in contact, or, between pedestrians in contact with the  
 121 walls. The expression for this force is  
 122

$$\mathbf{f}_g^{(ij)} = \kappa (r_{ij} - d_{ij}) \Theta(r_{ij} - d_{ij}) \Delta\mathbf{v}^{(ij)} \cdot \mathbf{t}_{ij} \quad (4)$$

123 where  $\kappa$  is a fixed parameter. The function  $\Theta(r_{ij} - d_{ij})$  is zero when its  
 124 argument is negative (that is,  $r_{ij} < d_{ij}$ ) and equals unity for any other case  
 125 (Heaviside function).  $\Delta\mathbf{v}^{(ij)} \cdot \mathbf{t}_{ij}$  represents the difference between the tan-  
 126 gential velocities of the sliding bodies (or between the individual and the  
 127 walls).

## 128 2.2. The inner stress model

129 As mentioned in Section 1, the “inner stress” stands for the cumulative  
 130 emotions that the pedestrian receives from his (her) neighbors. This mag-  
 131 nitude may change the pedestrian’s behavior from a relaxed state to panic,  
 132 and consequently, we propose that his (her) desired velocity  $v_d$  increases as  
 133 follows [4]

$$v_d(t) = [1 - M(t)] v_d^{\min} + M(t) v_d^{\max} \quad (5)$$

134 for  $M(t)$  representing the “inner stress” as a function of time. The minimum  
 135 desired velocity  $v_d^{\min}$  corresponds to the (completely) relaxed state, while the  
 136 maximum desired velocity  $v_d^{\max}$  corresponds to the (completely) panic state.  
 137

138 The inner stress  $M(t)$  in Eq. (5) is assumed to be bounded between zero  
 139 and unity. Vanishing values of  $M(t)$  mean that the pedestrian is relaxed,  
 140 while values approaching unity correspond to a very anxious pedestrian (*i.e.*

141 panic state).

142

143 The emotions received from the pedestrian's surrounding are responsible  
144 for the increase in his (her) inner stress  $M(t)$ . But, in the absence of stressful  
145 situations, some kind of relaxation occurs (say, the “stress decay”), attaining  
146 a decrease in  $M(t)$ . Following Ref. [8], a first order differential equation for  
147 the time evolution of  $M(t)$  can be assumed

$$\frac{dM}{dt} = -\frac{M}{\tau_M} + \mathcal{P} \quad (6)$$

148 Whenever the pedestrian receives alerting emotions from his (her) neigh-  
149 bors (expresses by the contagion efficiency  $\mathcal{P}$ ), the “inner stress” is expected  
150 to increase. But, if no alerting emotions are received, his (her) stress is ex-  
151 pected to decay according to a fixed relaxation time  $\tau_M$ . Thus, the first term  
152 on the right of Eq. (6) handles the settle down process towards the relaxed  
153 state. The second term on the right, on the contrary, increases his (her)  
154 stress towards an anxious state.

155

156 We assume that the parameter  $\mathcal{P}$  reflects the effect of the emotions re-  
157 ceived from alerting (anxious) neighbors within a certain radius, called the  
158 *contagion radius*. As described in Appendix Appendix A, if  $k$  pedestrians  
159 among  $n$  neighbors are expressing fear (see Fig. 1), then the actual value of  
160  $\mathcal{P}$  is

$$\mathcal{P} = J \left\langle \frac{k}{n} \right\rangle \quad (7)$$

161 where the parameter  $J$  represents an *effective contagion stress* (see Appendix  
162 A for details). This parameter resembles the pedestrian susceptibility to en-  
163 ter in panic. For simplicity we further assume that this parameter is the  
164 same for all the pedestrians.

165

166 The symbol  $\langle \cdot \rangle$  represents the mean value for any short time interval (see  
167 Appendix A for details). However, for practical reasons, we will replace this  
168 mean value with the sample value  $k/n$  at each time-step.

169

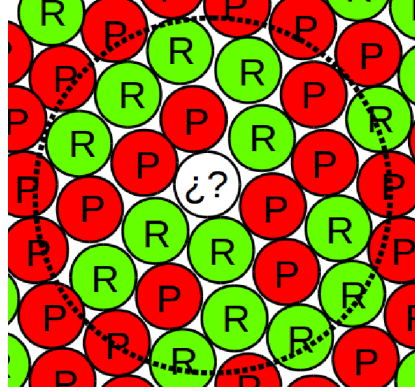


Figure 1: (Color on-line only) Crowd with relaxed (green circles) and panicking (red circles) pedestrians. The state of the pedestrian labeled with question marks depends of the amount of neighboring panicking and relaxed individuals (see Eq. 7). The circle indicate the contagious radius.

170 *2.3. The stress decay model*

171 The pedestrian “stress decay” corresponds to the individual’s natural re-  
172 laxation process in the absence of stimuli (*i.e.* emotions), until he (she) settles  
173 to the relaxed state. This behavior is mathematically expressed through the  
174 relaxation term in Eq. (6). Thus, in the absence of stimuli (that is, vanishing  
175 values of  $\mathcal{P}$ ), it follows from Eq. (5) and Eq. (6) that

176

$$v_d(t) = v_d^{\min} + (v_d^{\max} - v_d^{\min}) M(0) e^{-t/\tau_M} \quad (8)$$

177 for any fixed value  $M(0)$  at  $t = 0$ , and a vanishing value of  $M(t)$  long time  
178 after ( $t \gg \tau_M$ ). The characteristic time  $\tau$  for the desire force (see Section 2.1)  
179 is different from  $\tau_M$ . Ref. [6] suggests that  $\tau_M \simeq 50$  seconds.

180

181 The characteristic time  $\tau_M$  may be different from the suggested value  
182 according to specific environmental factors. Eq. (8) proposes the way to  
183 handle an estimation of  $\tau$  whenever the composure desired velocity  $v_d(t_c)$  is  
184 known ( $t_c$  being the time required to arrive to a relaxed state). Assuming  
185  $M(0) = 1$ , the corresponding expression of the inverse of the characteristic  
186 time  $\tau_M$  is

$$\tau_M^{-1} = \frac{1}{t_c} \ln \left( \frac{v_d^{\max} - v_d^{\min}}{v_d(t_c) - v_d^{\min}} \right) \quad (9)$$

187    *2.4. Topological characterization of the escaping pattern*

188    One of the most useful image processing technique is the computation of  
189    the Minkowski functionals. This general method, based on the concept of in-  
190    tegral geometry, uses topological and geometrical descriptors to characterize  
191    the topology of two and three dimensional patterns (Ref. [14]).

192

193    We used this method to analyze data (images) obtained from the video  
194    of the Charlottesville incident. So, we focused the attention on the 2-D case.  
195    Three image functionals can actually be defined in 2-D: area, perimeter and  
196    the Euler characteristic. The three can give a complete description of 2-D  
197    topological patterns appearing in (pixelized) black and white images.

198

199    To characterize a pattern on a black and white image, each black (or  
200    white) pixel is decomposed into 4 edges, 4 vertices and the interior of the  
201    pixel or square. Taking into account the total number of squares ( $n_s$ ), edges  
202    ( $n_e$ ) and vertices ( $n_v$ ), the area ( $A$ ), perimeter ( $U$ ) and Euler characteristic  
203    ( $\chi$ ) are defined as

$$A = n_s, \quad U = -4n_s + 2n_e, \quad \chi = n_s - n_e + n_v \quad (10)$$

204    The area is simply the total number of (black or white) pixels. The  
205    second and third Minkowski functionals describe the boundary length and  
206    the connectivity or topology of the pattern, respectively. The latter corre-  
207    sponds to the number of surfaces of connected black (white) pixels minus the  
208    number of completely enclosed surfaces of white (black) pixels (see Ref. [15]).

209

210    **3. Experimental data**

211    In this section we introduce two incidents, as examples of real life panic  
212    propagation. The first one occurred in Turin (Italy) while the other one took  
213    place in Charlottesville (USA) in 2017. We further present relevant data  
214    extracted from the corresponding videos available in the web (see on-line  
215    complementary material).

216

217    *3.1. Turin (Italy)*

218    On June 3rd 2017, many Juventus fans were watching the Champions  
219    League final between Juventus and Real Madrid on huge screens at Piazza

220 San Carlo. During the second half of the match, a stampede occurred when  
 221 one (or more) individuals shouted that there was a bomb. More than 1000  
 222 individuals were injured during the stampede, although it was a false alarm.  
 223 Fig. 2 captures two moments of the panic spreading (see caption for details).  
 224 The arrow in Fig. 2b points to the individual that caused the panic spread-  
 225 ing. He will be called the *fake bomber* throughout this investigation.  
 226



(a) Pedestrians watching the screen.



(b) Pedestrians in panic.



(c) Panic spreading.

Figure 2: (Color on-line only) (a) Snapshot of the crowd watching the football match. The screen is on the left (out of the scene). The pedestrians on the right are actually in fear due to the *fake bomber*. The (b) snapshot corresponds to the same scene as (a) but shifted to the state at 10 seconds right (actually, the camera appearing in this image is the one that captured the (a) image). The *fake bomber* appears in the scene and is indicated with a green arrow. (c) Analysis of the panic spreading among the crowd. The blue and orange profiles represent the relaxed and anxious pedestrians, respectively, associated to the (a) image (see text for details). In fact, in the (b) image we can observe (on the right of the image) the camera that captured the (a) image. The total number of contour bodies is  $N = 131$ .

227 The recordings from Piazza San Carlo show how the pedestrians escape  
 228 away from the “panic source”, that is, from the *fake bomber*. It can be seen  
 229 in Fig. 2b the opening around the panic source a few seconds after the shout.  
 230 The opening exhibits a circular pattern around the *fake bomber*. This be-

231 havior gradually slows down as the pedestrians realize the alarm being false.  
232 Approximately 20 seconds after the shout, the pedestrians calm down to the  
233 relaxed state while the opening closes.

234

235 In order to quantify the panic contagion among the crowd, we split the  
236 video into 14 images. The frame rate was 2 frames per second. Thus, the  
237 time interval between successive images was 0.5 seconds.

238

239 Fig. 2c shows the profile corresponding to the first image. Any (distin-  
240 guishable) pedestrian in Fig. 2a is outlined in Fig. 2c as a body contour. The  
241 contour colors represent the state of the pedestrians, relaxed pedestrians are  
242 outlined in blue (on-line version) and anxious pedestrians are outlined in  
243 orange (on-line version). The latter correspond to the individuals that sud-  
244 denly changed their motion pattern. That is, individuals that turned back  
245 to see what happened or pedestrians that were pushed towards the screen  
246 (on the left) due to the movement of his (her) neighbors.

247

248 The panic spreading shown in Fig. 2c occurs from right to left, until  
249 nearly all the contours bodies switch to the panic state (*i.e.* orange in the  
250 on-line version). Notice, however, that a few pedestrians may remain relaxed  
251 for a while, even though his (her) neighbors have already switched to the  
252 panic state. Or, on the contrary, pedestrians in panic may be completely  
253 surrounded by relaxed pedestrians, as appearing on the left of Fig. 2c. Both  
254 instances are in agreement with the hypothesis that pedestrians may switch  
255 to a panic state according to an *contagion efficiency*  $\mathcal{P}$ . See Appendix A for  
256 details on the  $\mathcal{P}$  computation within the contagion radius.

257

258 The inspection of successive images provides information on the new anx-  
259 ious or panicking pedestrians and the state of their current neighbors. Ap-  
260 pendix B summarizes this information, while detailed values for the contagion  
261 efficiency  $\mathcal{P}$  and the contagion stress  $J$  are reported in Table B.1. Notice that  
262 the data sampling is strongly limited by the total number of outlined pedes-  
263 trians (that is, 131 individuals). Thus, the reported values for  $t > 4$  s are  
264 not really suitable as parameter estimates because of the finite size effects.  
265 In order to minimize the size effects, we focused on the early stage of the  
266 contagion were the contagion stress  $J$  seems to be (almost) stationary (see  
267 Fig. B.14).

268

269        The (mean) contagion stress for the Turin incident was found to be  
270         $J = 0.1 \pm 0.055$  (within the standard deviation). This value appears to be  
271        surprisingly low according to explored values in the literature (see Ref. [8]).  
272        However, we shall see in Section 5 that this stress is enough to reproduce  
273        these real incidents.

274

275        *3.2. Charlottesville, Virginia (USA)*

276        One person was killed and 19 injured when a car ran into a crowd of pedes-  
277        trians during an antifascist protest (Charlottesville, August 12th, 2017). The  
278        incident took place at the crossing of Fourth St. and Water St. Fig. 3a shows  
279        a snapshot of the incident (the video is provided in the supplementary ma-  
280        terial).

281

282        In the video, we can see that the whole crowd gets into panic. But, we  
283        can identify two groups of pedestrians, according to the amount of informa-  
284        tion they have about the incident. The individuals near the car (say, less  
285        than 5 m) actually witnessed when the driver ran over into the crowd. How-  
286        ever, far away pedestrians become aware that something happened among  
287        the crowd due to the fear emotions of his (her) neighbors. But, they cannot  
288        determine the nature of the incident because the car is out of their sight.  
289        Thus, the pedestrians nearer to the car have more information than the far  
290        away individuals.

291

292        The video also shows that the pedestrians close to the car stop running as  
293        soon as the car stops. On the contrary, individuals located far away continue  
294        escaping after this occurs due to their lack of information.

295

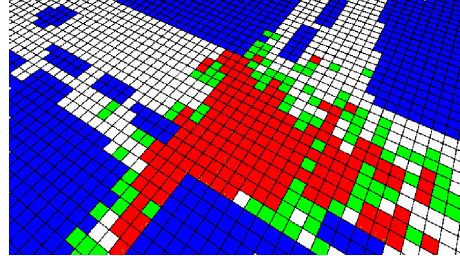
296        Using the program ImageJ [16], we followed the trajectories of various  
297        pedestrians. As shown in Fig. 4, most of the trajectories are approximately  
298        radial to the car. Notice, however, that three individuals ran toward the car  
299        to help the other injured pedestrians.

300

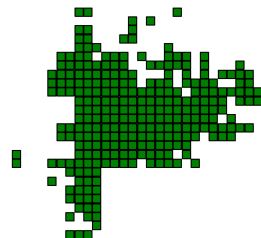
301        In order to obtain more experimental data, we split the video into 19  
302        frames. The frame rate was two frames per second. We further overlapped a  
303        square grid on each frame, but taking into account the two-point perspective  
304        of each image. Each cell was colored with different colors depending if it was  
305        occupied by pedestrians, obstacles, etc (see caption in Fig. 3b for details).



(a) Original frame.



(b) Pixelated image.



(c) Perspective correction.

Figure 3: (Color on-line only) (a) Image of the incident in Charlottesville. This image corresponds to the first frame of the video. (b) Pixelated image of the original frame. In the image we identify in blue color the obstacles, like cars and buildings. Green and red cells are occupied by one and more than one pedestrians, respectively. The street was colored in white. The line spacing was 12 pixels. The cell size was, approximately,  $1.5 \text{ m} \times 1.5 \text{ m}$ . (c) Perspective correction of the pixelated image. In green color we represent the position of the occupied cells by pedestrians. The white spaces represents the obstacles (buildings and cars) and the street.

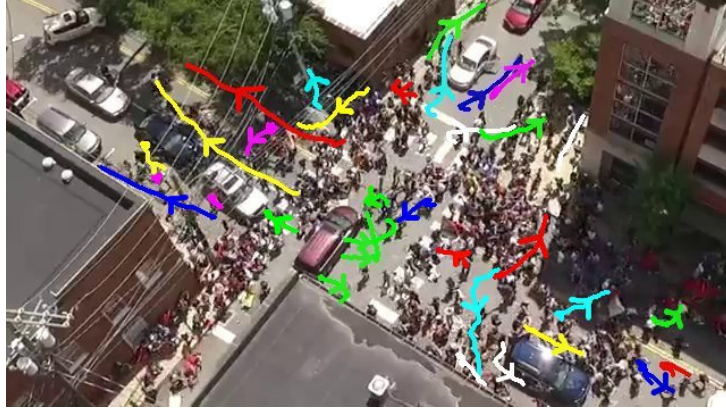


Figure 4: (Color on-line only) Trajectories for some pedestrians in panic from the Charlottesville video. The pedestrians' positions were recorded on consecutive images, and then joined by means of the software ImageJ. The arrows represent the movement direction.

306 Finally, we performed a back-correction of the perspective for a better in-  
307 spection of the grid. The result is shown in Fig. 3c.

308  
309 The complete analysis of the geometrical and topological patterns ap-  
310 pearing on the grid can be found in Section 5.  
311

#### 312 4. Numerical simulations

##### 313 4.1. The simulation conditions

314

##### 315 The Turin scenario

316 We mimicked the Turin incident (see Section 3) by first placing 925 pedes-  
317 trians inside a  $21\text{ m} \times 21\text{ m}$  square region. The pedestrians were placed in  
318 a regular square arrangement, meaning that the occupancy density was ap-  
319 proximately  $2\text{ people/m}^2$ . After their desire force was set (see below), the  
320 crowd was allowed to move freely until the system reaches the balance state  
321 before initiating the simulation. This balance situation can be seen in Fig. 5a  
322 and corresponds to the initial configuration for the panic spreading simula-  
323 tion.

324

325 The on-line blue line on the left of Fig. 5a represents the wide screen men-  
326 tioned in Section 3.1. We assumed that the pedestrians are attracted to the

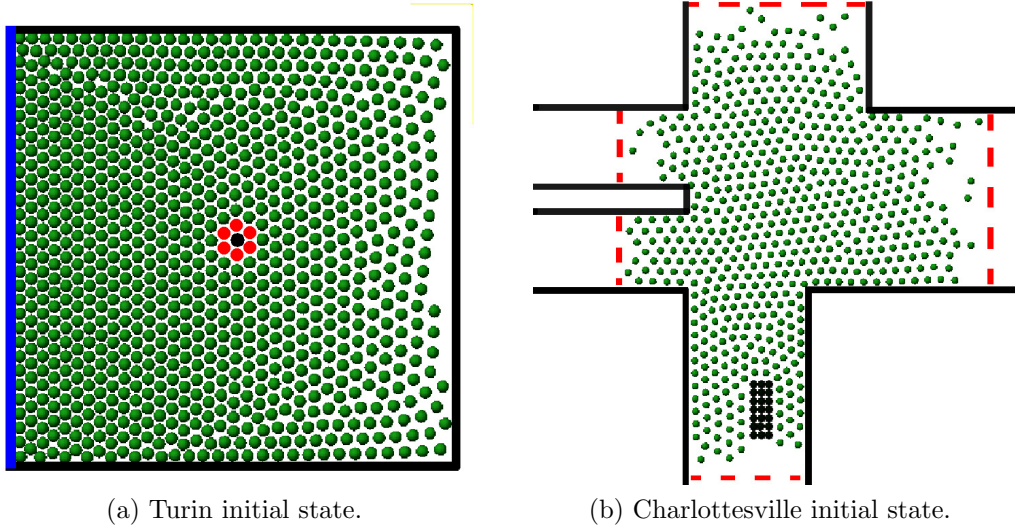


Figure 5: (Color on-line only) Snapshots of the initial configuration for the (a) Turin (Italy) and (b) Charlottesville (Virginia, USA) simulations. The relaxed pedestrians are represented in green circles on both images. (a) The *fake bomber* is represented in black, while his first neighbors are represented in red (see text for details). The blue line on the left represents the wide screen. (b) The car is represented by 21 black circles and moves from bottom to top. The solid (black) lines represent the walls and other obstacles (*i.e.* parked cars on the middle left of the image (see Fig. 3)). The width of the street at the bottom of the image is 8 m and at the top reaches 15 m (see red dashed lines). The street width on the left is divided into two paths of 5 m each, while the street width on the right is 13 m (see red dashed lines). Initially, the pedestrians were placed at random positions inside the region bounded by the red dashed lines.

327 screen in order to have a better view of the football match. Thus, a (small)  
328 desire force pointing towards the screen was included at the beginning of  
329 the simulation. This force equaled  $m v_d / \tau$  for the standing still individuals  
330 ( $v(0) = 0$ ), according to Eq. (2). We further assumed that the pedestrians  
331 were in a relaxed state at the beginning of the simulation, and therefore, we  
332 set  $v_d = 0.5 \text{ m/s}$  [12]. This value accomplished a local density that did not  
333 exceed the maximum expected for outdoor events, say,  $3\text{-}4 \text{ people/m}^2$ .

334

335 The pedestrian in black in the middle of the crowd in Fig. 5a represents  
336 the *fake bomber* appearing in the video. He is responsible for triggering the  
337 panic contagion at the beginning of the simulations. For simplicity, we as-  
338 sumed that he remained still during the panic spreading process.

339

340 The pedestrians in red in Fig. 5a are responsible for triggering the alert,  
341 as they are very close to the *fake bomber* (less than 1 m). They were initially  
342 set to the panic state in the simulation (see Section 4.2 for details).

343

344 Recall that the event takes place outdoor. Piazza San Carlo, however, is  
345 surrounded by walls (as can be seen in Fig. 2a). We considered along the  
346 simulations that the crowd always remained inside the *piazza* and no other  
347 pedestrian were allowed to get inside during the process.

348

#### 349 *The Charlottesville scenario*

350 The initial conditions for simulating the incident at Charlottesville are  
351 somewhat different from those detailed in Section 4.1. The pedestrians are  
352 now placed at random positions within certain limits around the street cross-  
353 ing (see Fig. 5b). But, in order to counterbalance the social repulsion between  
354 pedestrians, a (small) inbound desire force was set. That is, the pedestrian's  
355 desire force pointed to the center of the crossing.

356

357 The total number of pedestrians appearing in Fig. 5b is 600. This number  
358 was computed taking into account the total number of occupied cells and the  
359 amount of pedestrians per cell of the first frame of the video (see caption of  
360 Fig. 3b for details). Due to the low image quality of Fig. 3a, we were not  
361 able to distinguish if more than two pedestrians occupy a given cell. Thus,  
362 we simply assumed that each red cell was occupied by only two pedestrians.

363

364 After setting the pedestrian's desire force to  $v_d = 0.5$  m/s, we allowed  
365 them to move freely towards the center of the street crossing. This instance  
366 continued until a similar profile to the one in Fig. 3a was attained.

367

368 Then, we assumed, according to the video, that the pedestrians tried to  
369 stay at a fix position. Thus, we set the desired velocity to zero and allowed  
370 the system to reach the balance state before initiating the simulation. No-  
371 tice that this condition differed slightly from the Turin condition, where the  
372 desired velocity was set to 0.5 m/s due his (her) own desire to reaches the  
373 screen (see Section 4.1).

374

375 The "source of panic" for the Charlottesville's incident corresponds to  
376 the *offending driver* moving along the y direction in Fig. 5b. We modeled  
377 the *offending driver* as a packed group of 21 spheres, (roughly) emulating  
378 the contour of a car (see Fig. 5b). The mass of the packed group was set  
379 to 2000 kg. The car moved along the y direction at 3 m/s until it reached  
380 the center of the street intersection. When this occurred, it stopped and  
381 remained fix until the end of the simulation.

382

383 As in the Turin situation, we assumed that those pedestrians very close  
384 to the car (that is, less than 1 m) entered into panic immediately, and thus,  
385 they were initially set to the panic state. When the car stopped, the "source  
386 of panic" was switched off.

387

388 The streets are considered as open boundary conditions. This means that  
389 the pedestrians are able to rush away from the crossing as far as they can.

390

### 391 4.2. The simulation process

392 The videos that capture the panic spreading over the crowd let us classify  
393 the pedestrians into those moving relaxed or those moving anxiously. These  
394 are qualitative categories that can be easily recognized through the pedes-  
395 trian's behavioral patterns. An accurate value for the inner stress  $M$  seems  
396 not to be possible from the videos. Thus, we assume that the pedestrians  
397 may be in one of two possible states: relaxed or in panic. The former means  
398 that his (her) desired velocity does not exceed a fix threshold  $v_d^{\lim}$ , or  $M_{\lim}$ ,  
399 according to Eq. (5). The latter means that the individual surpassed this

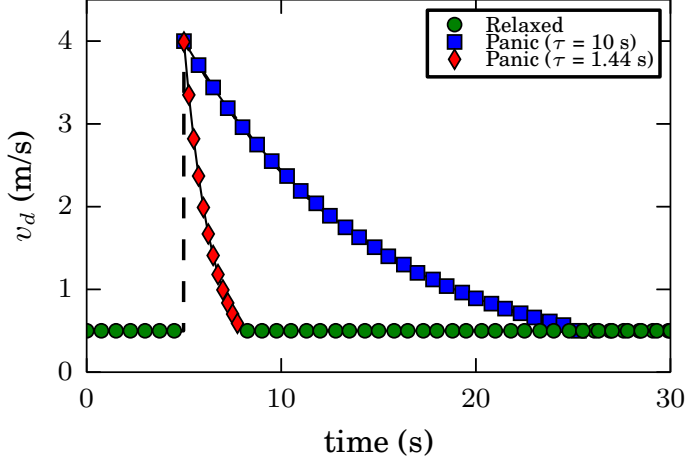


Figure 6: (Color on-line only) Time evolution of the desired velocity  $v_d$  for a single individual. The green color corresponds to the relaxed state, while the red color corresponds to the panic state. At  $t = 5$  s the  $v_d$  switches from 0.5 m/s to 4 m/s due to panic contagion. No further stimulus is received after the contagion. The desired velocity decays exponentially from  $t > 5$  s resembling the stress decay. The red diamond and blue square symbols represent two exponential characteristic times:  $\tau = 1.44$  s and  $\tau = 10$  s, respectively. At  $t \simeq 10$  s and  $t \simeq 25$  s (depending the value of  $\tau$ ) the desired velocity attains  $v_d^{\text{lim}} = 0.5$  m/s and the individual returns to the relaxed state.

400 threshold.

401

402 We already mentioned in Section 4.1 that the desired velocity  $v_d = 0.5$  m/s  
 403 is in correspondence with an accepted literature value for relaxed individuals  
 404 and the expected local density for approximately 900 individuals. Hence,  
 405 we set  $v_d^{\text{lim}} = 0.5$  m/s as a reasonable limit for the pedestrian to be con-  
 406 sidered relaxed. This limit is supposed to be valid for either the Turin and  
 407 the Charlottesville incident, since the total number of pedestrians involved in  
 408 each event and the expected maximum local density are similar in both cases.

409

410 For simplicity,  $v_d^{\min}$  and  $v_d^{\max}$  (Eq. (5)) were set to zero and 4 m/s, re-  
 411 spectively, in all the simulations. The maximum velocity  $v_d^{\max} = 4$  m/s cor-  
 412 responds to reasonable anxiety situations appearing in the literature [10, 11,  
 413 17, 18].

414

415 Fig. 6 illustrates the time evolution for the desired velocity  $v_d(t)$  of an

416 individual who switches from the relaxed state to the panic state (see caption  
417 for details). Notice that the increase in the inner stress is implemented as  
418 an (almost) instantaneous change in his (her) desired velocity due to panic  
419 contagion. Once in panic, however, the stress decay phenomenon applies, re-  
420 gardless of any other neighbor expressing fear. The stress decay stops when  
421 the individual settles to the relaxed state, that is, when the  $v_d$  returns back  
422 to 0.5 m/s. When this occurs, the pedestrian moves randomly at this desired  
423 velocity until the end of the simulation.

424

425 Notice that either in the Turin and the Charlottesville situation (see  
426 Fig. 4), the anxious pedestrians escapes radially from the source of panic.  
427 That is, from the *fake bomber* or the *offending driver*.

428

429 In order to determine the experimental value of the characteristic time  
430  $\tau$ , we measured the time required by an anxious pedestrian to recovers his  
431 (her) relaxed state ( $t_c$ ). According the analysis of the videos, in the Turin's  
432 case anxious pedestrians returns to a relaxed state after 20 seconds.

433

434 But, in the Charlottesville case, pedestrians near to the car (less than  
435 5 m) relaxed after 3 seconds. However, far away pedestrians arrive to the  
436 relaxed state after 20 seconds. Recall from Section 3.2, that individuals close  
437 to the car has more information about the incident nature than far away  
438 ones. Thus, when the car stops, near individuals recovers his relaxed state  
439 unlike the far away pedestrians that continues in panic.

440

441 We computed the experimental value of the characteristic time  $\tau$  for each  
442 scenario using Eq. (9) with  $v_d^{\min} = 0$  m/s,  $v_d^{\max} = 4$  m/s and  $v_d(t_c) = 0.5$  m/s.  
443 In the Turin's case,  $\tau$  equals, approximately, to 10 seconds, while in the Char-  
444 lottesville's case the characteristic time equals to 1.44 seconds and 10 seconds  
445 for pedestrians located close to the car or far away from it, respectively.

446

447 Notice that an anxious pedestrian has more or less "influence" over his  
448 neighbors according his (her) information level about the incident. That is,  
449 for example an individual near to the car can spread his (her) fear emotion  
450 over a relaxed pedestrian during, 3 seconds only. In other words, during the  
451 time that the pedestrians were in the state of panic ( $t_c$ ).

452

453    *The panic contagion process*

454    The panic contagion process was implemented as follows. First, we asso-  
455    ciated an effective contagion stress  $\mathcal{P}^{(i)}$  to each relaxed individual, according  
456    to Eq. (7). That is, we computed the fraction of neighbors in the panic state  
457    in his (her) vicinity within a fix contagion radius (2 m). Second, we switched  
458    the state of each relaxed individual to the panic state with probability  $\mathcal{P}^{(i)}$ .  
459    The  $\mathcal{P}^{(i)}$  values were updated at each time step (say, 0.05 s).

460

461    Notice that this contagion process may be envisaged as a Susceptible-  
462    Infected-Susceptible (SIS) process. The Susceptible-to-Infected transit cor-  
463    responds to the (immediate) increase of  $v_d$  from 0.5 m/s to 4 m/s (with effec-  
464    tive contagion stress  $\mathcal{P}^{(i)}$ ). The Infected-to-Susceptible transit corresponds  
465    to the stress decay from 4 m/s back to 0.5 m/s.

466

467    We want to remark the fact that the emotions received by an individual  
468    in the panic state were neglected, and thus, did not affect the stress decay  
469    process. This should be considered a first order approach to the panic con-  
470    tagion process.

471

472    *Simulation software*

473    The simulations were implemented on the LAMMPS molecular dynamics  
474    simulator [19]. LAMMPS was set to run on multiple processors. The cho-  
475    sen time integration scheme was the velocity Verlet algorithm with a time  
476    step of  $10^{-4}$  s. Any other parameter was the same as in previous works (see  
477    Refs. [17, 11]).

478

479    We implemented special modules in C++ for upgrading the LAMMPS  
480    capabilities to attain the “social force model” simulations. We performed  
481    between 60 and 90 simulations for each situation (see figures caption for  
482    details). Also, the processes lasted between 10 s and 20 s according each  
483    analysis. Data was recorded at time intervals of 0.05 s. The recorded mag-  
484    nitudes were the pedestrian’s positions and their emotional state (relaxed or  
485    anxious) for each evacuation process.

486

487    **5. Results**

488    In this section we discuss the results obtained from either real life situations  
489    and computer simulations. Two sections enclose these results in order  
490    to discuss them in the right context. We first analyze the Turin case (Section  
491    5.1), while the more complex one (Charlottesville, Virginia) is left to Section  
492    5.2.

493

494    *5.1. Turin*

495

496    *5.1.1. The contagion stress parameter*

497    As a first step, we measured the mean number of anxious pedestrians  
498    during the first 20 s of the escaping process for a wide range of contagion  
499    stresses ( $J$ ). This is shown in Fig. 7. As can be seen, the number of anxious  
500    pedestrians increases for increasing contagion stresses. That is, as pedestri-  
501    ans become more susceptible to the fear emotions from his (her) neighbors,  
502    panic spreads faster among the crowd.

503

504    The fraction of pedestrians that switch to the anxious state can be clas-  
505    sified into three qualitative categories as shown in Fig. 7. For  $J$  ranging be-  
506    tween 0 to 0.01, no significant spreading appears. But this scenario changes  
507    rapidly for the  $J$  (intermediate) range between 0.01 and 0.03. The slope in  
508    Fig. 7 displays a maximum throughout this interval. However, if the stress  
509    becomes stronger (say, above 0.03), the majority of the crowd enters into  
510    panic regardless of the precise value of  $J$ . A threshold for this is around  
511     $J = 0.04$ .

512

513    Notice that Fig. 7 is in agreement with the experimental Turin value for  
514    the mean contagion stress ( $J = 0.100 \pm 0.055$ , see Section 3). The panic  
515    situation at Piazza San Carlo, as observed from the videos, shows that all  
516    the pedestrians moved to the panic state. The snapshot in Fig. 2b illustrates  
517    the situation a while after the (fake) bomber called for attention.

518

519    The panic contagion shown in Fig. 7 does not appear to change signifi-  
520    cantly for increasing contagion radii. We explored situations enclosing only  
521    first neighbors (2 m) to situations enclosing as far as 6 m. Notice that  $J$  close  
522    to 0.025 seems to be an upper limit for any weak panic spreading situation, or

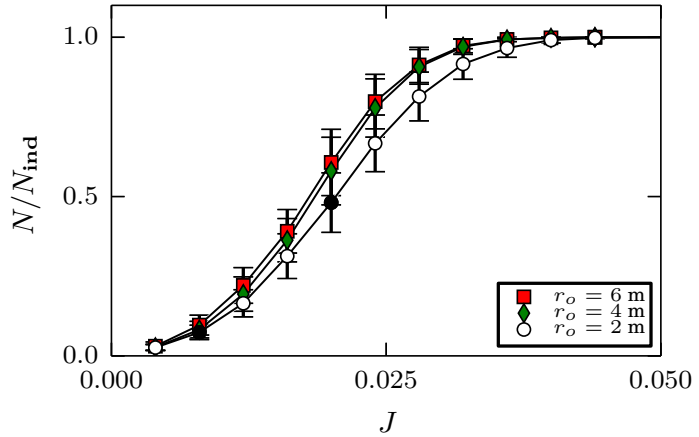


Figure 7: (Color on-line only) Normalized number of anxious pedestrians during the first 20 s of the escaping process as a function of the contagion stress  $J$  for  $r_o = 2$  m, 4 m and 6 m.  $N$  is the number of anxious pedestrians. The plot is normalized with respect to the total number of individuals ( $N_{ind} = 925$ ).  $J$ -values of 0.01 and 0.02 are indicated in black color (and circle symbols). Mean values were computed from 60 realizations. The error bars corresponds to  $\pm\sigma$  (one standard deviation).

523 the lower limit for any widely spreading situation. We may hypothesize that  
 524 two qualitative regimes may occur for the panic propagation in the crowd.

525

526 Following the above working hypothesis, we turned to study any morpho-  
 527 logical evidence for both regimes in Section 5.1.2 .

528

### 529 5.1.2. The morphology of the escaping pattern

530 Our next step was to examine the anxious pedestrian's spatial distri-  
 531 bution for the Piazza San Carlo scenario. The corresponding videos show  
 532 that the individuals tried to escape radially from the (fake) bomber (see  
 533 Fig. 2b). Thus, the polar space binning (*i.e.* cake slices) centered at the  
 534 (fake) bomber seemed the most suitable framework for inspecting the crowd  
 535 morphology at different pieces. We binned the *piazza* into  $N_{bins} = 30$  equally  
 536 spaced pieces as shown in Fig. 5a. The angle between consecutive bins was  
 537  $\varphi = 360^\circ/N_{bins} = 12^\circ$ .

538

539 Fig. 8 exhibits the number of bins or slices (normalized by the total num-

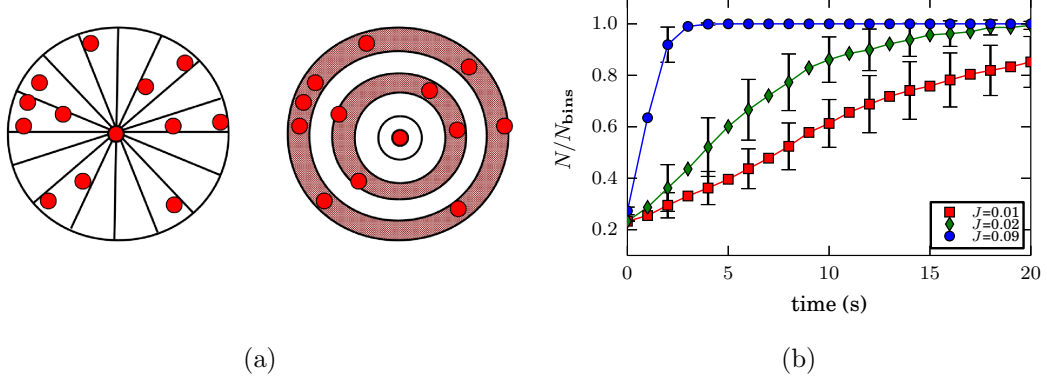


Figure 8: (Color on-line only) (a) Schematic representation of the radial (left) and circular (right) bins (see text for more details). The red circles represent the position of many anxious pedestrians. The fake bomber is place at the center of the region. (b) Fraction of occupied radial bins by anxious pedestrians vs. time (in seconds) for  $J = 0.01$ ,  $0.02$  and  $0.09$ .  $N$  is the number of occupied radial bins (see text for more details). The plot is normalized with respect to the total number of radial bins ( $N_{\text{bins}} = 30$ ). Mean values were computed from 60 realizations. The error bars corresponds to  $\pm\sigma$  (one standard deviation).

ber of bins) occupied *at least* by one anxious pedestrian. Three different contagion situations are represented there. These situations represent the qualitative categories mentioned in Section 5.1.1. That is,  $J = 0.01$  for low panic spreading,  $J = 0.02$  for an intermediate spreading and  $J = 0.09$  for wide panic spreading (see caption of Fig. 8 for details).

According to Fig. 8, the number of occupied bins (slices) increases monotonically during the escaping process. This means that panic propagates in all directions (from the bomber) until nearly all the slices become occupied. However, the slopes in Fig. 8 for each situation are quite different. As the contagion stress  $J$  increases, the bins become occupied earlier in time (higher slopes). For the most widely spread situation ( $J = 0.09$ ) all the slices become occupied before the first 5 seconds, meaning that we may expect escaping pedestrians in any direction during most of the contagion process.

Fig. 9 represents the aforementioned three situations after 15 s since the (fake) bomber shout (see caption for details). These snapshots may be easily compared with the corresponding slice occupancy plot exhibited in Fig. 8.

558  
559     Fig. 9a corresponds to the lowest contagion stress ( $J = 0.01$ ). We can  
560     see an amorphous “branching” pattern for those pedestrians in panic (red  
561     circles). From the inspection of the whole process through an animation,  
562     we further noticed that these configuration could be classified into two types  
563     (see below).

564  
565     A sharp “branching” profile is present in Fig. 9b for  $J = 0.02$ , although  
566     this category exhibits an extended number of pedestrians in panic. The high-  
567     est contagion stress category ( $J = 0.09$ ), instead, adopts a circular profile  
568     (see Fig. 9c).

569  
570     Both “branching” profile (amorphous and sharp) observed for  $J = 0.01$   
571     and  $J = 0.02$  (respectively) may be associated to the positive slopes in  
572     Fig. 8. Likewise, the circular profile for  $J = 0.09$  can be associated to the flat  
573     (blue) pattern therein. This suggests, once more, that two qualitative regimes  
574     may occur for the panic propagation in the crowd, as hypothesized in Sec-  
575     tion 5.1.1. Low contagion stresses correspond to the (qualitative) branch-like  
576     regime, while high contagion stress correspond to the (qualitative) circular-  
577     like regime. The snapshot in Fig. 2b clearly shows a circular-like regime, as  
578     expected for the obtained experimental value of  $J$ .

579  
580     The branching-like profile in Piazza San Carlo is not completely symmet-  
581     ric since the pedestrian’s density is higher near the screen area (on the left  
582     of Fig. Appendix B and Fig. 9) than in the opposite area. The pedestri-  
583     ans near the screen can not move away as easily as those in the opposite direc-  
584     tion. Thus, the panic contagion near the screen occurs among almost static  
585     pedestrians, while the contagion on the opposite area occurs among moving  
586     pedestrians. Both situations, although similar in nature, produce an asym-  
587     metric branching. We labeled as *passive* branching the one near the screen,  
588     and *active* branching the one in the opposite direction.

589  
590     It may be argued that since the  $J = 0.09$  pattern in Fig. 8 exhibits a  
591     positive slope at the very beginning of the contagion process and a vanishing  
592     slope a few seconds after (say, 5 s), the association of branch-like to low  $J$ ,  
593     and circular-like to high  $J$ , is somehow artificial. This is not true, as ex-  
594     plained below.

595

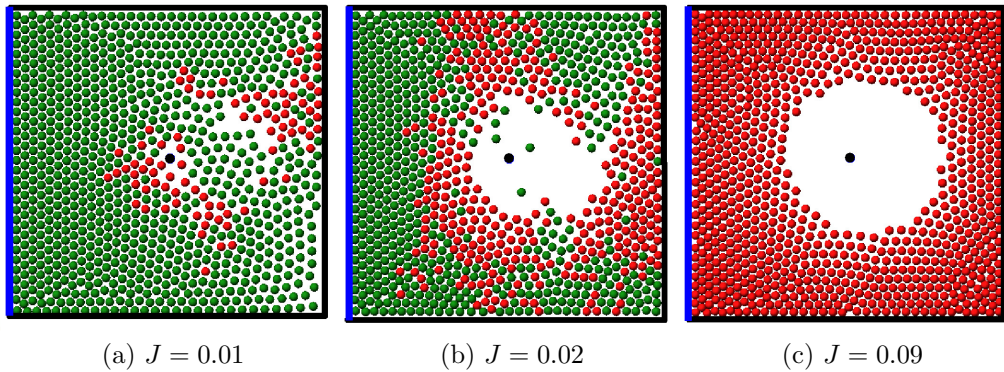


Figure 9: (Color on-line only) Snapshots of different escaping processes for three values of contagion stress in the first 15 seconds. The different colors of the circles represents the anxiety state of each pedestrian. Relaxed and panic pedestrians are represented in green and red circles, respectively. The *fake bomber* is placed at the center of the region and is represented in black circle. Relaxed pedestrians desire to reach the screen located on the left (blue line).

We further binned the *piazza* into circular sectors around the (fake) bomber as shown in Fig. 8 (see caption for details). We carried out a similar analysis as in Fig. 8, but for the sectors. Say, we computed the number of occupied sectors at each time-step. The results were similar as for the slices (not shown). This means that both (slices and sectors) behavioral patterns are strongly correlated (for any fixed  $J$ ).

The number of occupied sectors, somehow, indicates the speed of the radial propagation. Thus, the circular-like profiles correspond to higher speeds than the branch-like profiles, and consequently, it is not possible to associate low stress to circular profiles (or high stress to branch profiles). The propagation velocity will simply not match. Indeed, the circular profile appears only at high contagion stresses (for this *piazza* geometry).

We may summarize the investigation so far as follows. The panic spreading dynamic may experience important (qualitative) changes according to the “efficiency” of the alerting process between neighboring pedestrians. This is expressed by the contagion stress parameter  $J$ . Our simulations show that panic propagates weakly for low values of  $J$ . This produces a branch-like, slow panic spreading around the source of danger (for a simple geometry). However, if  $J$  exceeds (approximately) 0.025 the panic contagion spreads

617 freely in a circular-like profile (for a simple geometry). The propagation also  
618 becomes faster.

619

620 It should be emphasized that  $J \sim 0.025$  is an approximate threshold,  
621 but well formed circular-like profiles appear, in our simulations, for stresses  
622 above 0.03. Stresses beyond 0.04 exhibit similar profiles as those for  $J \sim 0.04$ .  
623 These results are valid for contagion radii between 2 m and 6 m.

624

625 The circular-like regime and the branch-like regime are consequence of  
626 two main factors: the radially escape away from the source of panic (see  
627 Section 4.2) and the fraction of pedestrians that switch to the anxious state.

628

629 For low values of contagion stress there are a small fraction of pedestrians  
630 that get into panic. In the escaping process, they have to avoid the majority  
631 of the crowd in a “random walk”. Others individuals in panic line up be-  
632 hind the first (*lane formation*) to minimize the efforts in the escaping process.

633

634 On the other hand, for the high contagion stress, the majority of the  
635 crowd enters into panic. Anxious pedestrians near the *fake bomber* escapes  
636 easily from his (her) due that also far away individuals run away too. So,  
637 they has not “resistance” from the crowd to escape from the source of panic.  
638 This is the reason for the circular-like pattern for high contagion stress.

639

640 Recall that the increase in the “inner stress” is the mechanism allow-  
641 ing the panic to spread among the crowd. The “emotional decay”, however,  
642 seems not to play a relevant role in Piazza San Carlo (and in our simulations).  
643 This is because the experimental characteristic time for the “emotional de-  
644 cay” is  $\tau = 10$  s, allowing anxious pedestrians to settle back to the relaxed  
645 state after 20 s (see Fig. 6).

646

647 Finally, we want to remark that although the Piazza San Carlo (Turin)  
648 situation attains a highly symmetrical situation with a well localized source  
649 of danger (*fake bomber*), our first approach was to consider a circular room  
650 with the source of danger at the center (not shown). All relaxed pedestrians  
651 tried to stay at a fix position while individuals in panic were able to escape  
652 radially outward from the fake bomber. The results from this simple scenario  
653 agreed with the Piazza San Carlo situation for high values of  $J$  (above 0.03).  
654 That is, the simulated crowd (in panic) adopted a circular pattern around

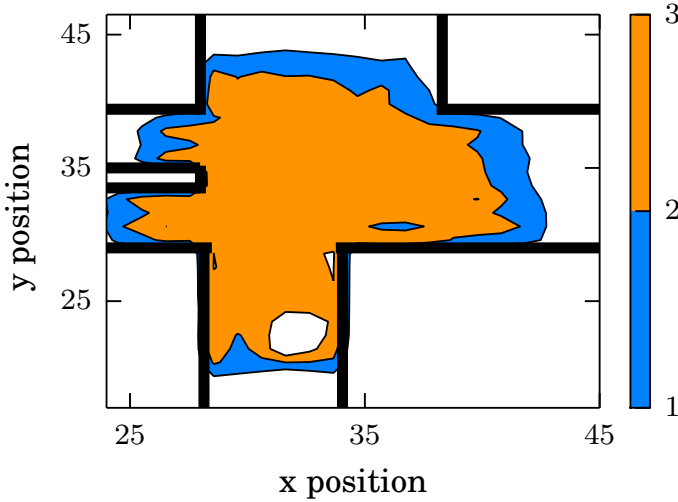


Figure 10: (Color on-line only) Mean density contour lines computed from 90 processes. This density map corresponds to the initial state of the Charlottesville simulation. The scale bar on the right is expressed in people/m<sup>2</sup>. The black lines represent the walls. The white circular shaped pattern at the bottom of the image corresponds to the car location. The contour lines were computed on a squared grid of 1.5 m × 1.5 m and then splined to get smooth curves. Level colors can be seen in the on-line version only.

655 the (fake bomber).

656

657 We will discuss in Section 5.2 a geometrically complex situation where  
658 either the “inner stress” and the “emotional decay” plays a relevant role.

659

660 *5.2. Charlottesville, Virginia*

661

662 *5.2.1. Density contour*

663 We first computed the discretized density pattern at the beginning of the  
664 simulation process in order to compare it with the video pattern shown in  
665 Fig. 3b. We used the same cell size as in Fig. 3b (1.5 m × 1.5 m). The corre-  
666 sponding contour density map can be seen in Fig. 10.

667

668 Fig. 10 and Fig. 3b exhibit the same qualitative profiles. Also, the pedes-  
669 trian occupancy per cell is similar on both figures. Notice that the middle

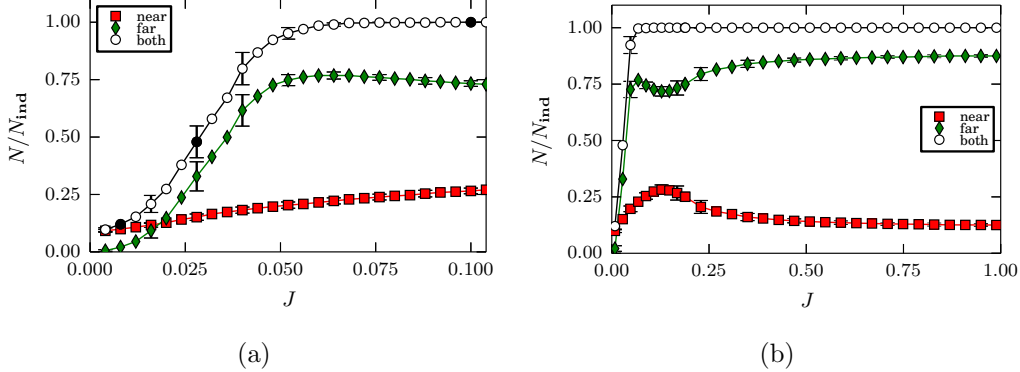


Figure 11: (Color on-line only) Normalized number of anxious pedestrians during the first 15 s of the escaping process, as a function of the contagion stress  $J$ .  $N$  is the number of anxious pedestrians. The plot is normalized with respect to the total number of individuals ( $N_{ind} = 600$ ). The red squares corresponds to panicking pedestrians close to the car (less than 5 m), while the green diamonds corresponds to those far away from the car (more than 5 m). The white circles correspond to the (normalized) set of all individuals in panic. Results for  $J = 0.010$ ,  $0.028$ , and  $0.1$  are indicated in black color (and circle symbols). Mean values were computed from 60 realizations. The error bars corresponds to  $\pm\sigma$  (one standard deviation).

of the region is occupied by two or more pedestrians per cell. The boundary cells, though, are occupied by a single pedestrian per cell in both figures. So, we may conclude that our initial configuration is qualitative and quantitative similar to the one in the video.

674

### 675 5.2.2. The contagion stress parameter $J$

676 Our next step was, as in the Turin case, to compute the mean number of  
 677 anxious pedestrians during the first 15 seconds of the escaping processes as  
 678 a function of the contagion stress ( $J$ ). The results can be seen in Fig. 11.  
 679

680 We observe that, likewise the Turin case, that the total number of anxious  
 681 pedestrians (circle symbols in Fig. 11) increases for increasing contagion  
 682 stresses. From the comparison between Fig. 7 and Fig. 11a we may realize  
 683 that both situations exhibit the same qualitative patterns for the total  
 684 number of anxious pedestrians. However, the slope for the Charlottesville  
 685 situation is somewhat lower with respect to the Turin situation (see Fig. 7).  
 686

687 In order to explain this slope discrepancy we computed, separately, the  
688 (mean) number of anxious pedestrians close to the car (*i.e.* source of panic)  
689 and those far away from the car. Recall from Section 4 that the former cor-  
690 respond to better informed pedestrians than the latter. The computation of  
691 the number of “near” anxious pedestrians actually include those pedestrians  
692 that get into panic very close to the car (less than 1 m).

693

694 We may recognize from Figs. 11a and 11b the same three qualitative cat-  
695 egories mentioned in Section 5.1.1, according to the contagion stress value.  
696 Notice, however, that the anxious pedestrians now settle to the relaxed state  
697 after 3 seconds (if near the car) or 20 seconds (if far away from the car). We  
698 will examine these regimes in the following sections.

699

#### 700 *The low contagion stress regime*

701 For  $J$  ranging between 0 to 0.02, most of the pedestrians that get anx-  
702 ious are close to the car, while pedestrians far away from the car remain in  
703 a relaxed state. This means that panic does not spread homogeneously over  
704 all the crowd.

705

706 Recall from Section 4.1 that individuals located very close to the car (less  
707 than 1 m) get into panic immediately. So, as the car moves across the crowd,  
708 the panic propagates first over these nearby individuals. This explains why,  
709 in Fig. 11a, there is a small number of anxious pedestrians for extremely low  
710 contagion stresses ( $J \sim 0$ ).

711

712 Notice that this small group of anxious pedestrians represent the first  
713 source of panic inside the crowd (regardless of the car). As the susceptibility  
714 to fear emotions increase, their neighbors get into panic. But, due to their  
715 rapid fear decay (3 seconds), their influence on the surrounding neighbors is  
716 low. This is the reason for the smooth increment of the near anxious pedes-  
717 trians.

718

719 Besides, we can observe from Fig. 11a that the number of far away pedes-  
720 trians getting into panic is not significant. Any pedestrian located far away  
721 from the car may only get anxious if panic surpasses his (her) contagion  
722 radius. So, if the number of “near” anxious pedestrians is low while also  
723 relaxing quickly (*i.e.* 3 seconds), then the “probability” that panic reaches

724 far away pedestrians from the car is indeed very low. This explains the low  
725 number of far away pedestrians that get anxious during this interval (less  
726 than 0.02).

727

728 *The intermediate contagion stress regime*

729 The panic spreading scenario changes if  $J$  ranges between 0.02 and 0.05.  
730 Along this interval, the total number of anxious pedestrians (white circles)  
731 increases abruptly. We can observe that this corresponds essentially to the  
732 increase in the amount of far away anxious pedestrians. Indeed, the number  
733 of near anxious pedestrians shown in Fig. 11a exhibits a smooth increment  
734 that cannot explain the abrupt increase of the total number of anxious indi-  
735 viduals.

736

737 Notice that an increment in the number of anxious “far away” pedestri-  
738 ans becomes possible (at high contagion stresses) due to the significant time  
739 window that they spend surrounded by other “far away” anxious pedestrians  
740 (say, 20 seconds). Thus, the compound effect of high susceptibility to fear  
741 emotions and the long lasting time decays ( $t_c$ ) explains the sharp increase in  
742 the number of anxious pedestrians.

743

744 *The high contagion stress regime*

745 Finally, if the contagion stress becomes intense (say, above 0.05), most  
746 of the individuals get into panic regardless of the precise value of  $J$ . Thus,  
747 as in the Turin situation, we may consider an approximate threshold for this  
748 regime around  $J = 0.07$ . Fig. 11b shows, however, that two noticeable be-  
749 haviors appear whether the contagion stress is (roughly) below  $J = 0.2$  or  
750 not (despite the fact that the majority enters into panic).

751

752 Below  $J = 0.2$ , the number of pedestrians that get into panic near the  
753 car increases for increasing contagion stresses, while above this threshold the  
754 corresponding slope in Fig. 11b changes sign. The number of far away anx-  
755 ious pedestrians exhibit, though, a small “U” shape and a positive slope for  
756  $J \gg 0.2$  (see Fig. 11b).

757

758 The increase in the number of individuals that get into panic near the car  
759 just below the threshold  $J = 0.2$  is a consequence of the increase in the sus-

760 susceptibility to fear emotions. But, above  $J = 0.2$ , the situation is somewhat  
761 different. The contagion stress is so intense that panic propagates rapidly  
762 into the crowd. People standing as far as 5 m from the car may switch to an  
763 anxious state, and thus, they get into panic *before* the car (*i.e.* the source  
764 of panic) approaches them. Our simulation movies (not shown) confirm this  
765 phenomenon. We further realized that many of the anxious individuals lo-  
766 cated near the car and computed in red squares in Fig. 11b at  $J \leq 0.2$  may  
767 actually move to the curve with green diamonds at extremely intense stresses  
768  $J \gg 0.2$ .

769

770 The above research may be summarize as follows. We identified three  
771 scenarios according to the contagion stress. If the susceptibility to fear emo-  
772 tions is low (below 0.02), the panic spreads over a small group of pedestri-  
773 ans located very close to the car. In the case of an intermediate contagion stress  
774 ( $J$  between 0.02 and 0.05), the number of pedestrians that get into panic far  
775 away from the car increases abruptly. Above  $J = 0.05$ , the panic spreads  
776 over all the crowd.

777

778 The propagation velocity of the fear among the crowd is related to the  
779 contagion stress ( $J$ ). As the susceptibility to fear emotions increases, the  
780 panic spreading velocity also increases. So, if pedestrians are very suscepti-  
781 ble to fear emotions, just a small number of individuals is capable of spreading  
782 panic over the whole crowd.

783

784 *5.2.3. The morphology of the escaping pattern*

785 In Section 5.2.2 we computed the total number of anxious pedestrians as a  
786 function of the contagion stress  $J$ . Now, we examine the pedestrian's spatial  
787 distribution. We computed the Minkowski functionals (area and perimeter)  
788 for different contagion stresses. The results are shown in Fig. 12.

789

790 The examined situations attain the same qualitative categories mentioned  
791 in Section 5.2.2. That is,  $J = 0.01$  for low panic spreading and  $J = 0.028$   
792 for an intermediate spreading, and the two cases ( $J = 0.1$  and  $J = 0.3$ ) for  
793 the highly intense situation. We also analyzed the limiting case ( $J = 1$ ). No  
794 distinction was made at this point between relaxed or anxious pedestrians.

795

796 Recall from Section 2.4, that the area is the number of occupied cells by,

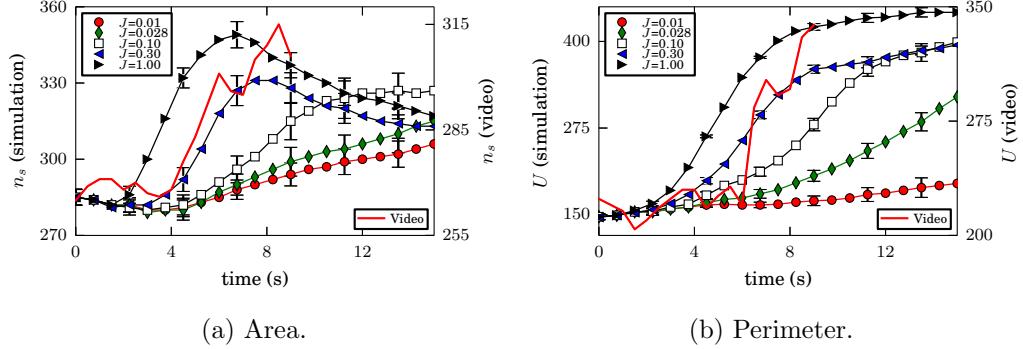


Figure 12: (Color on-line only) Minkowski functionals corresponding to the (a) area ( $n_s$ ) and (b) perimeter ( $U$ ) (see Section 2.4 for more details). Each symbol corresponds to the Charlottesville simulation. The red line corresponds to the experimental data extracted from the Charlottesville incident. In both cases, the cell area was  $1.5 \text{ m}^2$ . The duration of the Charlottesville video was 10 seconds. Mean values were computed from 90 realizations. The error bars corresponds to  $\pm\sigma$  (one standard deviation).

at least, one pedestrian. Fig. 12a shows two qualitatively different patterns, one before the first 4 seconds and the other one after this time period. The former exhibits a slightly negative slope, while a positive slope can be seen in the latter (at least for a short time period).

The first 4 seconds in the contagion process correspond to the time period since the car strikes against the crowd until it stops. So, we may associate the decrease in the area with the movement of the pedestrians next to the car. The process animations actually show that these individuals group themselves as the car moves towards the crowd.

The slope of the area changes sign after the first 4 seconds, meaning an increase of the occupied area (see Fig. 12a). This corresponds, according to our animations (not shown), to pedestrians running away from each other. The greater the contagion stress, the sharper the slope. Since these slopes represent the escaping velocity, Fig. 12a expresses the fact that people try to escape faster as they become more susceptible to fear emotions (at least during this short time period).

Fig. 12b exhibits the results for the computed perimeter. This functional informs us on the length of the (supposed) boundary enclosing the crowd.

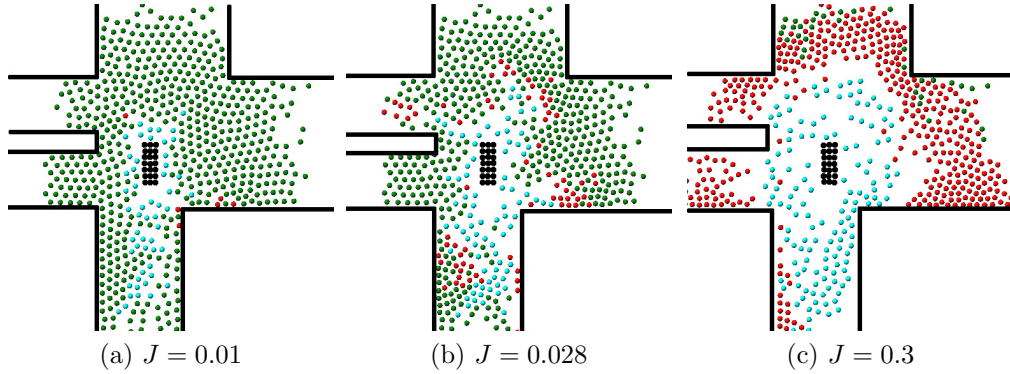


Figure 13: (Color on-line only) Snapshots of different escaping processes for low ( $J = 0.01$ ), intermediate ( $J = 0.028$ ) and high ( $J = 0.3$ ) contagion stress in the first 10 seconds. The different colors of the circles represents the anxiety state of each pedestrian. Relaxed and panic pedestrians are represented in green and red circles, respectively. The cyan circles represent the recovered pedestrians. That is, individuals that in the past were in panic but now are relaxed due to the stress decay. The *offending driver* is represented by black circles. The solid lines represent the walls and the row of cars located on the middle left of the image (see Fig. 3).

Unlike the area, the perimeter appears as an increasing function of time (for the inspected values of  $J$ ). Furthermore, as the susceptibility to fear emotions increases, the faster the perimeter widens.

The real life data included in Fig. 12 matches (qualitatively) the simulated patterns. Simulations corresponding to high contagion stresses appear to match better. The Minkowski functionals computed for  $J = 0.30$  exhibit the best matching patterns. Notice, however, that the scales of the experimental data and our simulations are different (see Fig. 12). This scale discrepancy is entirely due to the differences in the size of the occupancy cells corresponding to experimental data and to our simulations.

We finally examined the process animations for low ( $J = 0.01$ ), intermediate ( $J = 0.028$ ) and high ( $J = 0.3$ ) contagion stresses separately. These values correspond to the symbols in black color in Fig. 11. The complementary snapshots are shown in Fig. 13, captured after 10 seconds from the beginning of the process. We chose this time interval in order to differentiate the three situations more easily (see caption for details).

837     Fig. 13a corresponds to the lowest contagion stress ( $J = 0.01$ ). As al-  
838     ready shown from Fig. 11a, only a small number of pedestrians gets into  
839     panic (due the low susceptibility to fear emotions). These pedestrians are  
840     colored in cyan in Fig. 13a (on-line version only), and correspond to people  
841     standing close to the car path. No dramatic differences appear between the  
842     profiles shown in Fig. 5b and Fig. 13a. Thus, we may expect a smooth slope  
843     for the Minkowski functionals (see Fig. 12).

844

845     Fig. 13b shows a somewhat different scenario due to  $J = 0.028$  (the inter-  
846     mediate contagion stress). We realize that an increasing number of pedestri-  
847     ans are now in panic. Many pedestrians that appeared as relaxed in Fig. 13a,  
848     have now become anxious because of the fear emotions from the individuals  
849     located near the car. However, the occupied area did not change significantly  
850     from Fig. 13a. The perimeter, instead, is expected to increase because of the  
851     voids left back by the panicking pedestrians inside the crowd (see the red  
852     circles in the on-line version of Fig. 13b).

853

854     The more stressing scenario in shown in Fig. 13c. The whole crowd gets  
855     into panic for  $J = 0.3$ . This situation is comparable to the Turin incident  
856     (above  $J = 0.09$ ), despite the obvious geometrical differences. Thus, qual-  
857     itatively speaking, Fig. 4 and Fig. 13c show “similar” crowd profiles.

858

859     A few conclusions can be outlined from the above analysis. As in the  
860     Turin situation, we found different scenarios according the pedestrian’s sus-  
861     ceptibility to fear emotions. For low contagion stresses, the panic spreads  
862     over a small group of pedestrians standing close to the source of panic (the  
863     car). As the contagion stress ( $J$ ) increases, the influence of these nearby in-  
864     dividuals on their neighbors become more relevant. Thus, more pedestrians  
865     get into panic. If  $J$  is above 0.05, the fear spreads over all the crowd.

866

867     Despite the fact that above  $J = 0.05$  all the pedestrians becomes in  
868     panic, there are two qualitatively different regimes, bounded by a thresh-  
869     old at (roughly)  $J = 0.2$ . We found that below  $J = 0.2$ , the role of the  
870     pedestrians near the source of panic (say, the better informed pedestrians)  
871     is a relevant one, since they are the mean for propagating panic deep inside  
872     de crowd. But, above  $J = 0.2$ , the contagion stress is so intense that panic  
873     propagates rapidly into the crowd even though a minimum number of indi-  
874     viduals near the car get into panic.

876 **6. Conclusions**

877 We proposed a model in which panic spreads in a crowd according to a  
 878 epidemiological approach. In our work we have taken as experimental input  
 879 the information about two real panic-contagion events.

880

881 The contagion of panic offered a challenge to the emotional mechanism  
 882 operating on the pedestrians. We only included the “inner stress” and “stress  
 883 decay” as the main processes triggered during a panic situation. Although  
 884 the simplicity of this model, we attained fairly good agreement with the real  
 885 panic-contagion events.

886

887 We handled the coupling mechanism between individuals through the  
 888 contagion stress parameter  $J$ . This parameter appears to be responsible for  
 889 increasing the “inner stress” of the individuals. Our first achievement was  
 890 getting a real (experimental) value for  $J$ . The value for the Piazza San Carlo  
 891 event was  $0.1 \pm 0.055$ .

892

893 We further noticed through computer simulations that  $J$  controls the con-  
 894 tagion dynamics. The Piazza San Carlo event illustrates the dynamic arising  
 895 for high values of  $J$ , where everyone moves away from the source of stress.  
 896 However, this might not be the case for low values of  $J$ . Only a small number  
 897 of pedestrians will escape from danger, although many will roughly stay at  
 898 their current position. The whole impression will be like random “branches”  
 899 (the pedestrians in panic) moving away from the source of danger. We actu-  
 900 ally concluded that  $J \sim 0.03$  is roughly the limit between both dynamics.

901

902 Our simulations attained qualitatively correct profiles for the escaping  
 903 crowd for both the Piazza San Carlo and the Charlottesville street crossing.  
 904 But these profiles are geometry-dependent, and therefore, not a unique pro-  
 905 file could be established for any value of  $J$  at different incidents. We know  
 906 (for now) that geometries similar to Piazza San Carlo may produce branch-  
 907 like profiles ( $J < 0.03$ ) or circular-like profiles ( $J > 0.03$ ).

908

909 The “stress decay” depends on the nature of the source of panic (say,  
 910 whether if it corresponds to a fake alert or not) and the amount of informa-

911 tion that the pedestrians get from this source. That is, far away pedestrians  
912 from the igniting point of panic (fake bomber in the Turin situation, or the  
913 offending driver in the Charlottesville situation) may not have enough in-  
914 formation on the nature of the incident, but nearby pedestrians may get a  
915 more precise picture of the incident. The cleared this picture becomes to  
916 them, the faster they are allowed to settle down, and thus, the shorter the  
917 characteristic decay time.

918

919 We realized, however, that a shorter characteristic time actually prevents  
920 the panic from spreading. This was not the case at the Piazza San Carlo,  
921 since the fake bomber was not (directly) at the sight of the pedestrians (who  
922 were watching the football match). The Charlottesville incident, however,  
923 exhibited two groups of individuals, according to the available information.  
924 We noticed that the group near the source of danger attained a shorter  $\tau$   
925 than the others, preventing this group from escaping.

926

927 What we learned from the street crossing incident at Charlottesville is  
928 that the resulting pedestrian's dynamic is a consequence of the competing  
929 effects of the "inner stress" (increased by contagion stimuli) and the "stress  
930 decay". Both are essential issues for a trusty contagion model. The param-  
931 eters  $J$  and  $\tau$  appear as the most relevant ones within our model.

932

933 The  $J$  and  $\tau$  parameters may not always be available because of poor  
934 recordings or missing data. We experienced this difficulty with the video of  
935 the Charlottesville incident. But the experimental geometrical functionals,  
936 like the area or the perimeter, allowed the estimate of  $J$  by comparison with  
937 respect to simulated data ( $J \sim 0.3$ ).

938

939 We want to remark that different contagion radii (between 2 m and 6 m)  
940 did not produce significant changes on our simulations. This was unexpected,  
941 and thus, we may speculate that "spontaneous" contagion out of the usual  
942 contagion range may not produce dramatic changes, if the probability of  
943 "spontaneous" contagion is small.

944

945 **Acknowledgments**

946 C.O. Dorso is a main researcher of the National Scientific and Technical  
947 Research Council (spanish: Consejo Nacional de Investigaciones Científicas  
948 y Técnicas - CONICET), Argentina and full professor at Departamento de  
949 Física, Universidad de Buenos Aires. G.A. Frank is an assistant researcher  
950 of the CONICET, Argentina. F.E. Cornes is a PhD Student in Physics.

951

952 **Appendix A. The contagion efficiency**

953 Any individual among the crowd may increase his (her) anxiety level if  
954 his (her) neighbors are in panic. This is actually the propagation mechanism  
955 for panic: one or more pedestrians express their fear, alerting the others of  
956 imminent danger. The latter may get into panic and thus, a “probability”  
957 exists for getting into panic.

958

959 We hypothesize that the “probability to danger” (*contagion efficiency*)  
960 is the cumulative effect of the alerting neighbors. That is, if  $k$  pedestrians  
961 among  $n$  neighbors are expressing fear, then the contagion efficiency  $\mathcal{P}_n$  of  
962 an individual is

$$\mathcal{P}_n = p_n(1) + p_n(2) + \dots + p_n(n) \quad (\text{A.1})$$

963 where  $p_n(k)$  represents the contagion efficiency of  $k = 1, 2, \dots, n$  pedestri-  
964 ans (among  $n$  neighbors) expressing fear. The distribution for  $p_n(k)$  is a  
965 Binomial-like distribution if any neighbor expresses panic with fixed conta-  
966 gion efficiency  $p$ , regardless of the feelings of other neighbors. If the feelings  
967 of any neighbor (among  $n$  pedestrians) is not completely independent of the  
968 other neighbors,  $p_n(k)$  should be assessed as a Hypergeometric-like distribu-  
969 tion.

970

971 For the purpose of simplicity we assume that the Binomial-like distribu-  
972 tion is a valid approximation for the  $p_n(k)$  computation. Consequently,

$$\mathcal{P}_n = \sum_{k=1}^n \binom{n}{k} p^k (1-p)^{n-k} = 1 - (1-p)^n \quad (\text{A.2})$$

973 The mean value of neighbors expressing fear  $\langle k \rangle$  is  $np$ . Thus,

$$\mathcal{P}_n = 1 - \left(1 - \frac{\langle k \rangle}{n}\right)^n \quad (\text{A.3})$$

974 It is worth noting that this expression holds for a fix value of  $n$ . That  
975 is, the contagion efficiency  $\mathcal{P}_n$  is conditional to the amount of neighbor-  
976 ing individuals  $n$ . The contagion efficiency for any number of neighbors  
977  $n = 1, 2, \dots, M$  is

978

$$\mathcal{P} = \sum_{n=1}^M \mathcal{P}_n \pi_n \quad (\text{A.4})$$

979 where  $\pi_n$  means the contagion efficiency that there are  $n$  neighbors surround-  
980 ing the anxious pedestrian. Notice that the expression (A.4) neither includes  
981 the term for  $n = 0$ , nor the terms above  $M$ . The situation  $n = 0$  is not  
982 considered here since it corresponds to a “spontaneous” contagion to dan-  
983 ger. The situation  $n > M$  corresponds to far away individuals, and thus,  
984 not really capable of alerting of danger. The limiting value  $M$ , however, is  
985 supposed to be related to a pertaining distance and the the crowd packing  
986 density.

987

988 There is no available information on the values of  $\pi_n$ , although it may be  
989 written as the ratio  $\pi_n = z_n/M$  (number of current neighbors with respect  
990 to the maximum number of neighbors).

991

992 Recalling Eq. (A.3), the contagion efficiency  $\mathcal{P}_n$  may be expanded as

$$\mathcal{P}_n = 1 - (1 - np + \dots + p^n) = p f_n(p) \quad (\text{A.5})$$

993 The function  $f_n(p)$  stands for the summation

$$f_n(p) = n - \frac{n(n-1)}{2} p + \dots + p^{n-1} \quad (\text{A.6})$$

994 Each contributing terms in  $f_n(p)$  may be envisage as the alert to danger  
995 due to groups of individuals of increasing size (for a fix number of neighbors  
996  $n$ ). Notice, however, that the expression (A.6) holds if the feelings between  
997 neighboring pedestrians are completely independent. Otherwise, the func-  
998 tion  $f_n(p)$  should be considered unknown.

999

1000      The overall contagion efficiency reads

$$\mathcal{P} = \sum_{n=1}^M \frac{z_n}{M} \frac{\langle k \rangle}{n} f_n(p) \simeq J \left\langle \frac{k}{n} \right\rangle \quad (\text{A.7})$$

1001      where  $J$  represents an *effective stress* for the propagation, since it expresses  
1002      in some way the efficiency of the alerting process. That is, no panic propaga-  
1003      tion will occur for vanishing values of  $J$ , while the pedestrian susceptibility  
1004      to fear emotions will become more likely as  $J$  increases. The stress  $J$  may  
1005      depend, however, on the probability  $p$ . Appendix Appendix B shows that  
1006      this dependency is weak enough to be omitted in a first order approach.

1007

1008      The fraction  $\langle k/n \rangle$  corresponds to the mean fraction of neighbors express-  
1009      ing fear with respect to the total number of neighbors. This mean fraction  
1010      is computed over all the possible number of neighbors, according to Eq. (A.7).

1011

## 1012      **Appendix B. The sampling procedure for Turin**

1013      The effective stress  $J$  may be evaluated from any real life situation. De-  
1014      tails on the sampling procedure for the Turin incident at Piazza San Carlo  
1015      are given in Section 3.1.

1016

1017      As a first step, we identified those individuals that switched to the panic  
1018      state along the image sequence. We also identified the surrounding pedestri-  
1019      ans for each anxious individual, and labeled them as neighboring individuals  
1020      (regardless of their current anxiety state). For simplicity, we used the same  
1021      profile (shown in Fig. 2c) throughout the image sequence.

1022

1023      The mean fraction  $\langle k/n \rangle$  was obtained straight forward from this data.  
1024      Table B.1 exhibits the corresponding results (see second column).

1025

1026      Notice that the surrounding pedestrians actually correspond to the most  
1027      inner ring of pedestrians enclosing the anxious individual, but not the ones  
1028      within a certain radius. This radius, however, can be estimated from the  
1029      (mean) packing density of the crowd.

1030

Table B.1: Data provided from the Turin video (see Section 3.1 for details). Samples were taken at 0.5 s time intervals. The second column shows the number of pedestrians  $n_p$  that switched to the panic state at the corresponding time stamp. The third column exhibits the (mean) ratio between neighbors in panic with respect to the surrounding neighbors. The fourth column corresponds to the contagion efficiency  $\mathcal{P}$  computed as a “no-replacement” procedure (see text). The last column corresponds to the *contagion stress*  $J$  computed from the third and fourth columns. The total number of individuals was  $N = 131$ .

$t$	$n_p$	$\langle k/n \rangle$	$n_p/(N - N_p)$	$J$
0.5	1	0.17	0.0077	0.0453
1.0	1	0.20	0.0077	0.0385
1.5	5	0.43	0.0391	0.0909
2.0	5	0.42	0.0406	0.0967
2.5	2	0.13	0.0169	0.1300
3.0	4	0.55	0.0345	0.0627
3.5	6	0.36	0.0536	0.1489
4.0	13	0.64	0.1226	0.1916
4.5	11	0.68	0.1183	0.1740
5.0	10	0.52	0.1219	0.2344
5.5	22	0.63	0.3055	0.4849
6.0	29	0.90	0.5800	0.6444
6.5	15	0.88	0.7143	0.8117

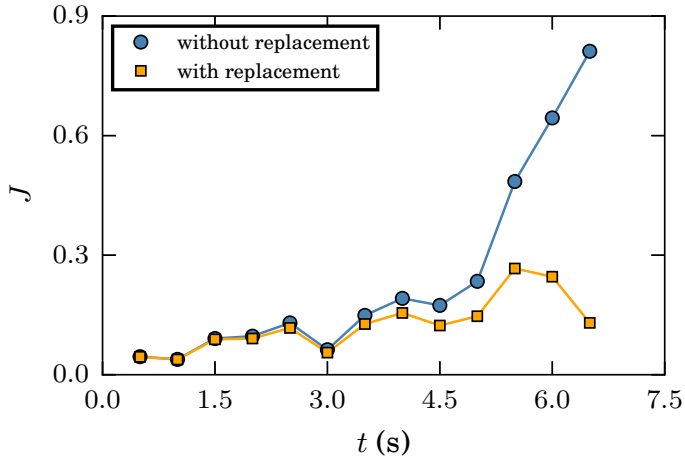


Figure B.14: (Color on-line only) The contagion stress  $J$  as a function of time  $t$  in seconds (see text for details). The rounded symbols (in blue color) correspond to the  $J$  values computed from a crowd of  $N = 131$  individuals and a sampling procedure “without replacement” (see Table B.1 for details). The squared symbols correspond to the  $J$  values computed from the same crowd, but following a sampling procedure “with replacement”. The mean stress for  $0.5 \text{ s} \leq t \leq 4 \text{ s}$  is  $J = 0.1 \pm 0.055$ .

1031     The anxious pedestrians at the border of the examined area of Piazza  
 1032     San Carlo (see ) are not included in Table B.1 since it was not possible to  
 1033     identify *all* of their surrounding pedestrians.

1034     The fraction of the anxious pedestrians  $n_p$  to the total number of in-  
 1035     dividuals  $N$  is a suitable estimate for the overall contagion efficiency  $\mathcal{P}$ .  
 1036     However, as panic propagates, the acknowledged anxious pedestrians  $n_p$  di-  
 1037     minish because the number of previously relaxed individuals reduces inside  
 1038     the analyzed area. Thus, the estimate of  $\mathcal{P}$  follows a sampling “without re-  
 1039     placement” procedure. That is, the fraction estimate is  $n_p/(N - N_p)$ , where  
 1040      $N_p$  corresponds to the number of individuals in panic until the previous time  
 1041     step.  
 1042

1043     Fig. B.14 shows the effective stress  $J$  computed as the ratio between  $\mathcal{P}$   
 1044     and  $\langle k/n \rangle$ . The contagion efficiency  $\mathcal{P}$  was estimated either as  $n_p/(N - N_p)$   
 1045     (*i.e.* without replacement) or  $n_p/N$  (*i.e.* with replacement). It can be seen  
 1046     that the sampling effects can be neglected for  $t \leq 4 \text{ s}$ .  
 1047

1048

1049 The  $J$  estimates exhibited in Fig. B.14 are not completely stationary  
 1050 along the interval  $0.5\text{ s} \leq t \leq 4\text{ s}$ . However, the increasing slope is not relevant  
 1051 for a first order approach. The mean value for the effective stress along  
 1052 this interval is  $J = 0.1 \pm 0.055$ .

1053

1054 **References**

- 1055 [1] D. Volchenkov, S. Sharoff, On the application of the dynamical systems theory to social modeling, in: P. Blanchard, R. Lima, L. Streit,  
 1056 R. V. Mendes (Eds.), *The Sciences of Complexity: From Mathematics*  
 1057 to Technology to a Sustainable World, Vol. CD-ROM, ZiF - Center for  
 1058 Interdisciplinary Research, 2001.
- 1060 [2] H. Zhao, J. Jiang, R. Xu, Y. Ye, Sirs model of passengers' panic  
 1061 propagation under self-organization circumstance in the subway emergency,  
 1062 *Mathematical Problems in Engineering* 2014 (2014) 608315.  
 1063 doi:<http://dx.doi.org/10.1155/2014/608315>.
- 1064 [3] L. Fu, W. Song, W. Lv, S. Lo, Simulation of emotional contagion using  
 1065 modified sir model: A cellular automaton approach, *Physica A: Statistical  
 1066 Mechanics and its Applications* 405 (Supplement C) (2014) 380 –  
 1067 391. doi:<https://doi.org/10.1016/j.physa.2014.03.043>.
- 1068 [4] L. Fu, W. Song, W. Lv, X. Liu, S. Lo, Multi-grid simulation of  
 1069 counter flow pedestrian dynamics with emotion propagation, *Simulation Modelling  
 1070 Practice and Theory* 60 (Supplement C) (2016) 1 – 14.  
 1071 doi:<https://doi.org/10.1016/j.simpat.2015.09.007>.
- 1072 [5] G. Chen, H. Shen, G. Chen, T. Ye, X. Tang, N. Kerr, A new kinetic  
 1073 model to discuss the control of panic spreading in emergency, *Physica  
 1074 A: Statistical Mechanics and its Applications* 417 (2015) 345 – 357.  
 1075 doi:<https://doi.org/10.1016/j.physa.2014.09.055>.
- 1076 [6] X.-H. Ta, B. Gaudou, D. Longin, T. Ho, Emotional contagion model for  
 1077 group evacuation simulation, *Informatica* 41 (2017) 169–182.

- 1078 [7] N. Pelechano, J. Allbeck, N. Badler, Controlling individual agents in  
 1079 high-density crowd simulation, Proceedings of the 2007 ACM SIG-  
 1080 GRAPH/Eurographics Symposium on Computer Animation (2007) 99–  
 1081 108.  
 1082 URL <https://repository.upenn.edu/hms/210>
- 1083 [8] A. Nicolas, S. Bouzat, M. N. Kuperman, Statistical fluctuations in  
 1084 pedestrian evacuation times and the effect of social contagion, Phys.  
 1085 Rev. E 94 (2016) 022313. doi:10.1103/PhysRevE.94.022313.  
 1086 URL <https://link.aps.org/doi/10.1103/PhysRevE.94.022313>
- 1087 [9] D. Helbing, I. Farkas, T. Vicsek, Simulating dynamical features of escape  
 1088 panic, Nature 407 (2000) 487–490.
- 1089 [10] D. Helbing, P. Molnár, Social force model for pedestrian dynamics, Phys-  
 1090 ical Review E 51 (1995) 4282–4286.
- 1091 [11] G. Frank, C. Dorso, Room evacuation in the presence of an obstacle,  
 1092 Physica A 390 (2011) 2135–2145.
- 1093 [12] D. Parisi, C. Dorso, Microscopic dynamics of pedestrian evacuation,  
 1094 Physica A 354 (2005) 606–618.
- 1095 [13] F. Cornes, G. Frank, C. Dorso, High pressures in room evacuation pro-  
 1096 cesses and a first approach to the dynamics around unconscious pedes-  
 1097 trians, Physica A: Statistical Mechanics and its Applications 484 (2017)  
 1098 282 – 298. doi:<https://doi.org/10.1016/j.physa.2017.05.013>.
- 1099 [14] C. O. Dorso, P. A. Giménez Molinelli, J. A. López, Topological char-  
 1100 acterization of neutron star crusts, Phys. Rev. C 86 (2012) 055805.  
 1101 doi:10.1103/PhysRevC.86.055805.  
 1102 URL <https://link.aps.org/doi/10.1103/PhysRevC.86.055805>
- 1103 [15] K. Michielsen, H. D. Raedt, Integral-geometry morphological  
 1104 image analysis, Physics Reports 347 (6) (2001) 461 – 538.  
 1105 doi:[https://doi.org/10.1016/S0370-1573\(00\)00106-X](https://doi.org/10.1016/S0370-1573(00)00106-X).
- 1106 [16] Rasband, W.S., ImageJ, U. S. National Institutes of Health, Bethesda,  
 1107 Maryland, USA, <https://imagej.nih.gov/ij/>, 1997-2016, Imagej.  
 1108 URL <https://imagej.nih.gov/ij/>

- 1109 [17] G. Frank, C. Dorso, Evacuation under limited visibility, International  
1110 Journal of Modern Physics C 26 (2015) 1–18.
- 1111 [18] I. M. Sticco, F. E. Cornes, G. A. Frank, C. O. Dorso, Be-  
1112 yond the faster-is-slower effect, Phys. Rev. E 96 (2017) 052303.  
1113 doi:10.1103/PhysRevE.96.052303.  
1114 URL <https://link.aps.org/doi/10.1103/PhysRevE.96.052303>
- 1115 [19] S. Plimpton, Fast parallel algorithms for short-range molecular dy-  
1116 namics, Journal of Computational Physics 117 (1) (1995) 1 – 19.  
1117 doi:<http://dx.doi.org/10.1006/jcph.1995.1039>.